Updated analysis of the ^{170}Er(p,t) ^{168}Er reaction data

D. Bucurescu* and S. Pascu
Horia Hulubei National Institute of Physics and Nuclear Engineering, Bucharest, Romania

G. Graw, R. Hertenberger, and H.-F. Wirth
Fakultät für Physik, Ludwig-Maximilians-Universität München, Garching, Germany

T. Faestermann
Technical University of Munich, Physics Department, D85748 Garching, Germany

R. Krücken
Lawrence Berkeley National Laboratory, Nuclear Science Division, Berkeley, California 94720, USA

M. Mahgoub
Physics Department, Jazan Universitym 45142 Jazan, Saudi Arabia
and Department of Physics, Sudan University of Science and Technology, PO Box 407, Khartoum, Sudan

J. Jolie, P. von Brentano,† and S. Heinze
Institut für Kernphysik, Matematisch-Naturwissenschaftliche Fakultät, Universität zu Köln, 50937 Köln, Germany

O. Möller
Institut für Kernphysik, Technische Universität Darmstadt, D-64289 Darmstadt, Germany

R. F. Casten
Wright Lab, Yale University, New Haven, Connecticut 06520, USA

D. A. Meyer Brittingham
Department of Physics and Astronomy, Agnes Scott College, Decatur, Georgia 30030, USA

(Received 28 February 2023; revised 20 May 2023; accepted 29 June 2023; published 10 July 2023)

More than 200 states up to 4.1 MeV excitation have been populated in ^{168}Er with the ^{170}Er(p,t) reaction at 25 MeV incident energy. About 80 of these states, with 0^+ and 2^+ assignments, were reported in a previous publication [D. Bucurescu *et al.*, Phys. Rev. C **73**, 064309 (2006)]. The present work considerably enriches the knowledge of this nucleus. A multistep coupled-channels analysis of the angular distributions is now presented for all the states observed in this experiment. Spin and parity values between 0^+ and 7^- are newly assigned for more than 100 states. For the states already reported in the ENSDF database with J^π values there is a good agreement with our values. The ^{168}Er nucleus remains one of the best experimentally known nuclei for states with low and medium spins below 4 MeV excitation energy, representing a challenge for future microscopic structure model calculations aiming to disentangle the contributions of different excitation degrees of freedom.

DOI: 10.1103/PhysRevC.108.014310

I. INTRODUCTION

Direct transfer nuclear reactions represent an important source of information on nuclear structure. When performed with high-energy resolution, one may identify a large number of excited states with low to medium spins in nuclei, and even uniquely determine their spin and parity. Many such studies were performed at the MLL (Maier-Leibnitz Laboratory of LMU Munich and TU Munich) MP tandem accelerator ([1–9]; the list is not exhaustive), using the Q3D magnetic spectrograph and an excellent, very high-resolution position-sensitive focal plane detector [10]. A campaign of (p,t) reaction experiments was initiated in 2005 with a study of eight nuclei in the rare-earth region. The main interest at that moment was to identify the 0^+ states in these nuclei, which are easy to recognize due to their strong forward peaking, and corroborate their distribution in excitation energy with the quantum phase transition from this region [2,3].

*bucurescu@nipne.ro
†Deceased.

The nucleus ^{168}Er was part of this set of nuclei, and results concerning the identification of 0^+ and 2^+ states up to 4.0 MeV excitation were published soon after these first papers, with an attempt to understand a large number of states with these spins based on different theoretical models [4]. The number of states assigned as 0^+ and 2^+ was more than 80, representing less than half of all the excited states that were observed in this study, i.e., more than 200. A more detailed analysis of these data was meanwhile performed, and results concerning the assignment of a large number of states with spins between $1\hbar$ and $7\hbar$ are reported in this paper. These results considerably enrich the number of low-lying states with known spin-parity in this nucleus.

II. EXPERIMENTAL DETAILS

The experiment was performed at an incident energy of 25.0 MeV. Angular distributions were measured at 7 angles between 5° and 37.5° in the laboratory system. Experimental details are given in our previous work [4]. The target was Er_2O_3, 120 μg/cm^2 thick deposited on 13 μg/cm^2 carbon backing, and had the following isotopic composition: 98% ^{170}Er, 1.1% ^{168}Er, 0.4% ^{167}Er, and 0.5% ^{166}Er. The most important peak impurities clearly observed in the 10° spectrum were the ground and 2_1^+ states of ^{166}Er from the (p,t) reaction on ^{168}Er (Fig. 1 of Ref. [4]. The ground state of ^{164}Er (from the ^{166}Er impurity) was not observed. Concerning the ^{167}Er impurity, it was known that the state with $L=0$ most strongly excited in the (p,t) reaction is the $7/2^+$, $E_x = 465$ keV one in ^{165}Er [11]. The peak corresponding to this state should have been observed around an excitation energy of 2100 keV in ^{168}Er, about 15 keV different from the 2114 keV state reported as 0^+ in ^{168}Er [4]. Because the difference in the Q values of the two reactions is known with an accuracy of 1.5 keV, the 2114 keV state cannot be confused with that from the ^{167}Er target impurity.

A number of 213 excited states were observed up to an excitation energy of 4.075 MeV, with an average energy resolution of around 6 keV. The measurements at each angle were performed with three different settings of the magnetic field of the Q3D spectrograph, in such a way that the resulting spectra had overlaps in energy: 0 to 1.53 MeV, 1.4 to 2.95 MeV, and 2.5 to 4.08 MeV. The energy calibration of the spectra was achieved by comparing with spectra measured under similar conditions for the ^{172}Yb(p,t) and ^{208}Pb(p,t) reactions (see [4]). Most of the finally adopted excited states were observed in the energy spectra measured at all seven angles, allowing the measurement of meaningful angular distributions. Missing points usually correspond to the absence of a peak at the right energy in the results of the automatic spectra fitting program, mostly due to its small intensity.

III. ANALYSIS OF THE ANGULAR DISTRIBUTIONS

To determine the transferred angular momentum (L) and spin ($J = L$) of a state populated through the (p,t) reaction, the shape of its experimental angular distribution is compared with that calculated with the code CHUCK3 [12]. The CHUCK3 code is able to calculate both one-step processes (from the initial state directly to the final state) by using the distorted-wave Born approximation (DWBA), in which the scattering problem is solved to first order in the interaction potential, and multistep processes, in which the final state can be reached by intermediate states, by using coupled-channels (CC) calculations. In the CC calculations the solution of the coupled equations related to the involved states is solved to all orders of the interaction potential. CHUCK3 can take into account up to eight channels (states) and up to 500 couplings between the channels.

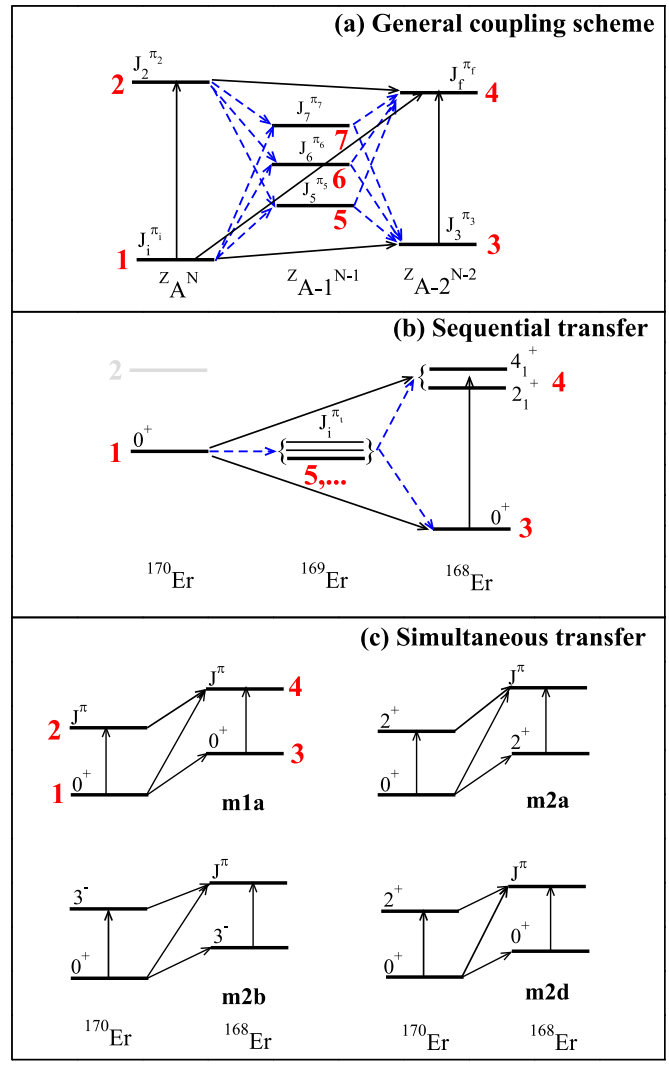

FIG. 1. Coupling schemes used in the CHUCK3 coupled-channels calculations. (a) General coupling scheme for a (p,t) reaction, involving seven channels (states); see text for comments. The seven channels are numbered 1,2,...,7 for reference in the text. (b) A simplified scheme highlighting the sequential transfer for the ^{170}Er(p,t) ^{168}Er reaction. For reasons explained in the text, channel 2 is not considered here. Note that this scheme is not purely sequential, but it includes some other transitions that may compete with the sequential ones (simultaneous direct $1 \rightarrow 4$ and two-step $1 \rightarrow 3 \rightarrow 4$ transfers). (c) Simultaneous transfer schemes for ^{170}Er(p,t) ^{168}Er, with the notation names of [7]. See Table I for the assignment of coupling schemes to particular levels.

TABLE I. Energy levels of ^{168}Er from the (p,t) reaction experiment, compared to the levels adopted in ENSDF [18]. The ENSDF levels are given in columns 1 and 2. Only levels with spin less than $8\hbar$ are shown. The levels previously assigned as 0^+ and 2^+ [2,4] are shown in columns 3 and 4, but they also appear in columns 1 and 2 because they were adopted by ENSDF. All the other levels from the present analysis are given in columns 3 and 5. Column 6 gives the differential cross section measured at 10° for all levels observed in the (p,t) reaction and column 7 the cross section integrated over the available angular range (usually 5° to 37.5°; see the angular distribution figures). The last column gives the coupling scheme used for the CHUCK3 calculations [see Fig. 1(c)]. The one-step DWBA calculations are labeled by 1sdw.ij, with (ij) denoting the transferred neutron orbital configurations (f: $f_{7/2}$; h: $h_{11/2}$, and h9 for $h_{9/2}$; i: $i_{13/2}$). The multistep coupled-channels calculations are specified by the label of the used coupling scheme [Fig. 1(c)] followed by the (ij) configuration, e.g., the notation m1a.ff means the coupling from Fig. 1(c), top left, and the two particles in the $2f_{7/2}$ orbit. For the levels with ambiguous J^π assignment (e.g., for the 2690.8 keV level), the coupling schemes corresponding to the possible J values of column 5 are specified. Figures 3 to 7 show the angular distributions in the (p,t) reaction of all the levels analyzed in the present work (not all the levels firmly assigned as 0^+ and 2^+ in the previous work [4] were included in the present analysis). For some of the levels analyzed in [4] and reanalyzed in this work, the J^π of [4] was crossed out in column 4 and replaced by the new assignment shown in column 5.

ENSDF Ref. [18]		^{170}Er(p,t) ^{168}Er expt.					
Energy (keV)	J^π	Energy (keV)	J^π Ref. [4]	J^π present	$d\sigma/d\Omega(10°)$ (μb/sr)	$\sigma_{\text{integr.}}$ (μb)	Obs.
0.00	0^+	0.1*1*	0^+		584 *7*	270 *5*	
79.804 *1*	2^+	79.8 *1*	2^+	2^+	155 *4*	64 *2*	m1a.ff
264.0888 *14*	4^+	264.1 *1*	4^+	4^+	47 *1*	39.8 *7*	m1a.ff
548.7470 *20*	6^+	548.7 *1*		6^+	3.3 *2*	3.6 *2*	m2a.ii
821.1685 *16*	2^+	821.2 *1*	2^+		27.6 *4*	14.9 *4*	
895.7947 *17*	3^+	895.8 *2*		3^+	0.7 *1*	1.9 *1*	m2a.ii
928.3020 *25*	8^+						
994.7474 *16*	4^+	994.5 *2*		4^+	19.3 *4*	15.5 *4*	m1a.ff
1094.0383 *16*	4^-						
1117.5703 *16*	5^+						
1193.0251 *17*	5^-	1193.0 *2*		5^-	5.4 *2*	6.2 *3*	1sdw.fi
1217.169 *14*	0^+	1217.1 *1*	0^+		7.9 *2*	5.6 *3*	
1263.9047 *19*	6^+	1264.0 *1*		(6^+)	1.8 *1*	1.2 *1*	m2a.ii
1276.2716 *20*	2^+	1276.3 *1*	2^+		3.0 *2*	1.9 *2*	
1311.4606 *17*	6^-						
1358.899 *5*	1^-	1358.7 *2*		1^-	2.6 *1*	2.0 *2*	m2b.hi
1403.7357 *23*	$(2)^-$	1402.6 *7*		2^-	0.1 *1*	0.4 *1*	m2b.ff
1411.0959 *18*	4^+	1409.9 *8*		4^+	0.2 *1*	0.3 *1*	m1a.ff
1422.12 *3*	0^+	1421.9 *2*	0^+		5.9 *3*	4.0 *3*	
1431.466 *4*	3^-	1431.5 *3*		3^-	9.7 *2*	9.0 *4*	1sdw.fi
1432.9508 *23*	7^+						
1448.9555 *17*	7^-	1448.7 *2*		(7^-)	2.9 *1*	5.1 *2*	m2b.fi
1493.133 *5*	2^+	1493.0 *2*	2^+		5.4 *2*	3.4 *2*	
1541.5564 *18*	3^-	1541.7 *5*		3^-	0.6 *1*	0.4 *1*	m2a.fi
1541.7094 *24*	$(4)^-$						
1569.4527 *25*	$(2)^-$						
1574.117 *4*	5^-	1574.0 *4*		5^-	3.3 *1*	4.7 *2*	1sdw.fi
1605.8503 *23*	8^-						
1615.3420 *18*	4^-						
1616.8060 *19*	6^+	1617.7 *5*		$(1^- + 6^+)$	1.2 *1*	0.8 *1*	doublet, 1sdw.hi,1sdw.ii
1624.507 *4*	8^+						
1629.698 *6*	$4^-, 5^-, 6^-$						
1633.4627 *23*	3^-	1633.4 *2*		3^-	11.9 *5*	11.1 *5*	1sdw.fi
1653.5486 *21*	3^+						
1656.274 *5*	$(4)^+$	1654.7 *5*		4^+	1.0 *1*	1.5 *1*	m1a.ff
1707.9929 *17*	5^-	1708.1 *5*		5^-	0.7 *1*	1.0 *1*	1sdw.fi
1719.1786 *24*	4^-	1718.5 *8*		(4^-)	0.4 *1*	0.3 *1*	m2b.ff
1736.6881 *20*	4^+	1736.7 *2*		4^+	10.7 *2*	10.6 *3*	1sdw.ff
1760.760 *3*	$(6)^-$						
1764.0 *4*							
≈1768.17							
1773.205 *3*	$(6)^-$						

TABLE I. (*Continued.*)

ENSDF Ref. [18]		^{170}Er(p,t) ^{168}Er expt.					
Energy (keV)	J^π	Energy (keV)	J^π Ref. [4]	J^π present	$d\sigma/d\Omega(10^\circ)$ (μb/sr)	$\sigma_{\text{integr.}}$ (μb)	Obs.
1780.00 *15*	9^-						
		1780.3 *4*		6^+	0.8 *1*	1.3 *2*	m2a.ii
1786.123 *14*	1^-	1786.4 *3*		(1^-)	1.4 *1*	1.5 *2*	m2b.hi
1795.325 *11*	(7^-)						
		1795.4 *3*		(5^-)	0.9 *1*	1.2 *1*	m2b.fi
1812.5 *16*	$(2^+, 3, 4^+)$						
1820.1321 *18*	6^-						
1820.476 *3*	5^-	1820.5 *3*		(5^-)	2.5 *1*	2.0 *1*	m2b.hi
1828.0639 *20*	3^-						
1833.54 *11*	0^+	1833.7 *2*	0^+		4.9 *2*	2.4 *2*	
1839.3474 *20*	5^+						
1848.354 *4*	2^+	1848.2 *2*	2^+		3.1 *1*	2.3 *2*	
1881.82 *3*							
1892.9346 *20*	(4^-)						
1893.100 *6*	2^+	1893.0 *2*	2^+		1.7 *1*	1.1 *1*	
1896.379 *3*	$(7)^-$						
1902.696 *7*	(6^+)	1902.7 *4*		(6^+)	0.6 *1*	0.9 *1*	m2a.ii
1905.0922 *25*	(4^-)						
1913.92 *3*	3^-	1913.6 *3*		3^-	1.3 *1*	1.7 *1*	1sdw.fi
1915.502 *4*	$(3)^+$						
1930.391 *4*	2^+	1930.1 *3*	2^+		0.5 *1*	0.4 *1*	
1936.596 *10*	1^-	1936.2 *6*		1^-	1.0 *1*	0.6 *1*	1sdw.hi
1949.636 *3*	$(6)^-$						
1950.8067 *20*	7^-						
1952.2 *7*	2^+	1952.2 *7*	2^+		0.8 *1*	0.8 *1*	
1961.3992 *20*	6^+	1960.6 *5*		(6^+)	1.0 *1*	1.0 *1*	m2a.ii
1972.314 *14*	$(2)^-$						
1983.0398 *24*	5^-	1982.4 *4*		5^-	0.4 *1*	0.7 *1*	m2b.hi
1994.821 *4*	$(3)^+$						
1999.2239 *22*	$(3)^-$						
2001.953 *4*	5^-	2001.6 *3*		$3^- + 5^-$	1.2 *1*	1.5 *7*	doublet, 1sdw.fi
2002.465 *4*	$(4)^+$						
2022.358 *21*	$(3)^-$	2022.3 *3*		3^-	0.6 *1*	0.8 *1*	1sdw.fi
2031.097 *7*	$(4)^+$						
2038.66 *20*	(8^-)						
2055.914 *8*	$(4)^+$	2055.8 *3*		4^+	1.9 *1*	2.4 *2*	1sdw.ff
2059.9751 *20*	$(4)^-$						
2080.457 *3*	$(4)^+$	2080.1 *4*		4^+	1.0 *1*	1.2 *1*	m1a.ff
2089.348 *3*	4^-						
2091.272 *5*	$(6)^-$						
2097.571 *6*	4^-						
2100.361 *4*	7^+						
2108.987 *4*	$(5)^+$						
2114.1 *4*	0^+	2114.1 *4*	0^+		1.3 *1*	0.7 *1*	
2118.791 *5*	$(6)^-$						
2122.428 *3*	$(5,6,7)^-$						
2125.427 *4*							
2129.246 *21*	$(5)^-$	2129.8 *23*			$\approx$0.2	$\approx$0.2 *2*	
2133.767 *15*	(1^+)						
2135.9 *7*	1^-						
2137.08 *9*	$(2)^+$						
2144.53 *3*							
2148.3685 *23*	5^-	2148.5 *7*		5^-	0.2 *1*	0.2 *1*	m2b.fi
2169.516 *12*	$(5)^+$						
2174.59 *8*		2174.0 *8*		(6^+)	1.0 *1*	1.0 *1*	m2a.ii

TABLE I. (*Continued.*)

ENSDF Ref. [18]		^{170}Er(p,t) ^{168}Er expt.					
Energy (keV)	J^π	Energy (keV)	J^π Ref. [4]	J^π present	$d\sigma/d\Omega(10^\circ)$ (μb/sr)	$\sigma_{\text{integr.}}$ (μb)	Obs.
2177.79 *8*	(2^+)						
2185.11 *3*	$(5)^-$	2185.5 *3*		5^-	1.5 *2*	2.5 *2*	1sdw.fi
2186.741 *4*	$(3)^+$						
2188.408 *10*	(5^+)						
2188.74 *16*	$(2^+, 3, 4^+)$						
2193.19 *4*	2^+	2193.0 *3*	2^+		12.2 *3*	9.2 *3*	
2200.4193 *23*	$(5)^-$						
2200.6 *4*	0^+	2200.6 *4*	0^+		0.4 *2*	0.4 *1*	
2210.016 *6*	(7^-)						
2218.5 *16*							
2221							
2230.30 *4*	$(2)^-$	2232.2 *3*		2^-	0.8 *1*	1.4 *2*	m2b.ff
2238.179 *3*	$(4)^+$						
		2238.1 *5*		1^-	1.3 *1*	1.0 *2*	m2b.hi
2243.514 *19*	$(3)^+$						
2246.530 *9*	$(6)^+$						
2249.68 *5*							
2254.754 *24*	(2^+)						
2254.84 *5*	$(3)^+$						
2255.343 *3*	$(6)^-$	2255.6 *5*		6^-	1.1 *1*	2.5 *2*	m2b.h9h9
2262.691 *7*	$(3)^-$	2262.8 *3*		3^-	1.9 *2*	2.4 *2*	1sdw.fi
2264 *4*	(0^+)						
2267.632 *8*	$(3,4,5)^+$						
2269 *5*	3^-						
2270.46 *5*							
2273.67 *9*	$(2^+, 3, 4^+)$						
2279.630 *5*	$(4)^+$	2279.5 *3*		4^+	1.5 *1*	1.4 *2*	m1a.ii
2286 *5*							
2294.0 *10*							
2298.260 *4*	$(4,5,6)^+$	2299.2 *4*		(5^+)	0.4 *1*	1.0 *1*	m2a.h9h9
2302.666 *4*	$(3)^-$						
2303.10 *3*	$(6)^-$						
2306.882 *24*	(6^+)						
2311.07 *3*	$(4)^+$	2311.2 *3*		4^+	3.9 *2*	4.7 *2*	1sdw.ff
2322.2 *2*	2^+	2322.2 *2*	2^+		9.6 *3*	7.9 *3*	
2323.01 *5*	3^-						
2331.987 *3*	6^-						
2336.26 *10*	4^+						
2337.100 *20*	3^-	2337.4 *2*		3^-	11.4 *3*	10.2 *3*	m2d.fi
2341.78 *24*	1						
2346.20 *9*	$1^-, 2^-, 3^-$						
2348.581*18*	4^-						
2349.3 *3*		2349.3 *3*	2^+		20.3 *4*	11.6 *3*	
2361.40 *19*	1						
2365.196 *14*	$(5)^-$						
2365.33 *12*	(1^+)						
2366.2 *2*	0^+	2366.2 *2*	0^+		13.4 *3*	4.9 *3*	
2368.585 *9*	(5^+)						
2373.657 *18*	2,3	2373.9 *6*		(1^-)	1.24 *17*	1.0 *2*	m2b.hi
2378.12 *8*							
2382.587 *4*	(2^+)						
2392.1 *2*	(0^+)	2392.1 *2*	(0^+)	0^+	3.7 *2*	2.5 *2*	m2a.h9h9
2392.118 *7*	$(5, 6^+)$						
2392.927 *9*	$(3^-, 4^+)$						
2393.71 *9*	(2^+)						

TABLE I. (*Continued.*)

ENSDF Ref. [18]		^{170}Er(p,t) ^{168}Er expt.					
Energy (keV)	J^π	Energy (keV)	J^π Ref. [4]	J^π present	$d\sigma/d\Omega(10^\circ)$ (μb/sr)	$\sigma_{\text{integr.}}$ (μb)	Obs.
2398.52 *9*	$(3^+, 4, 5^+)$						
2401.94 *24*	(1^-)						
2402.29 *7*	(4^-)						
		2405.5 *5*		6^+	1.5 *1*	2.5 *2*	m2a.ii
2411.795 *25*	$(5)^+$						
2417.02 *20*	$1^{(-)}$	2416.8 *7*			0.8 *1*	0.4 *2*	
2423.25 *9*							
2424.91 *6*	$(2)^+$	2424.1 *3*	2^+	2^+	8.2 *3*	7.1 *3*	m1a.ff
2427.2 *6*							
2434.659 *5*							
2440.054 *20*	$(4^+, 5^+)$						
2440.46 *5*	(2^+)						
2450.5 *3*	2^+	2450.5 *3*	(2^+)		4.2 *2*	4.1 *2*	prob. doublet
2451.165 *24*	(5^-)						
2455.96 *6*	$(3^+, 4, 5^+)$						
2458.7 *4*	1						
2461.8 *2*	2^+	2461.8 *2*	2^+		4.9 *2*	3.7 *2*	
2468.8 *9*							
2474.10 *6*	(6^-)						
2477.20 *6*	$(5)^-$	2477.5 *3*		(5^-)	7.7 *3*	10.8 *3*	m2b.h9i
2478.08 *7*	$(3)^-$						
2484.52 *6*	(3^+)						
		2485.9 *4*		(5^-)	4.3 *3*	6.9 *3*	m2b.hi
2486 *5*	3^-						
		2492.2 *5*			1.9 *2*	2.1 *3*	
2493.5 *3*	1^+						
2494.528 *15*	$(3)^-$						
2499.1 *5*							
2510.72 *24*	$1^{(-)}$	2511.1 *4*		1^-	1.2 *1*	1.0 *2*	m2b.hi
2513.67 *5*	$(4)^-$						
2517.48 *20*	$(3^+, 4^+)$						
		2518.5 *6*		(3^-)	0.4 *1*	0.6 *1*	1sdw.fi
2526.583 *12*	$(5)^-$	2526.9 *4*		(5^-)	1.9 *2*	2.5 *2*	m2b.hi
2527.78 *7*							
2528.80 *10*	$(5)^-$						
2538.1 *5*	2^+	2538.2 *5*	2^+		10.0 *3*	7.9 *3*	
2540.22 *5*	$(3,4,5)^+$						
2547.25 *7*	(4^+)						
2551.48 *7*	$(4,5)^-$						
2552.7 *4*	2^+	2552.3 *3*	2^+		3.0 *2*	2.5 *2*	
2558.66 *5*	$(5)^-$						
2561.56 *5*	(4^+)	2561.4 *2*		4^+	11.5 *3*	11.1 *3*	1sdw.ff
2563.5 *5*							
2571.31 *5*							
2572.5 *2*	0^+	2572.5 *2*	0^+		46.2 *6*	25.7 *6*	
2578.8 *5*							
		2580.4 *4*		2^+	10.8 *12*	9.4 *14*	1sdw.ff
2586.2 *6*		2585.5 *5*		1^-	1.8 *2*	1.3 *2*	m2b.hi
2594.4 *10*							
2601.2 *4*							
		2605.5 *4*		6^+	0.7 *3*	1.5 *7*	m2a.ii
2617.4 *2*	0^+	2617.4 *2*	0^+		23.6 *3*	9.4 *12*	
2626.3 *10*							
2628.57 *22*	$(3^+, 4, 5^+)$						
2629.2 *4*							

TABLE I. (*Continued.*)

ENSDF Ref. [18]		^{170}Er(p,t) ^{168}Er expt.					
Energy (keV)	J^π	Energy (keV)	J^π Ref. [4]	J^π present	$d\sigma/d\Omega(10^\circ)$ (μb/sr)	$\sigma_{\text{integr.}}$ (μb)	Obs.
		2631.4 *4*		1^-	7.1 *2*	4.4 *5*	1sdw.hi
2637.2 *10*							
2643.71 *13*	$1^{(+)}$						
2644.1 *6*	(0^+)	2644.1 *6*	~~0+~~	1^-	2.8 *2*	1.8 *3*	1sdw.hi
2651.9 *5*		2651.4 *6*		1^-	2.5 *4*	1.5 *2*	1sdw.hi
2656.86 *5*							
2657.66 *4*	(2,3,4)						
		2658.5 *9*		(4^+)	8.3 *4*	6.9 *5*	m1a.ff
2660.59 *7*	$(3,4)^+$						
2663.229 *20*	$(4)^+$						
2672.1 *5*	$(4^+, 5, 6^+)$						
		2673.6 *6*		5^-	1.2 *3*	3.2 *4*	m2b.hi
2676.3 *4*	1^+						
2683.8 *3*	(2^+)	2683.2 *4*		2^+	10.6 *2*	10.0 *4*	1sdw.ff
2689.0 *4*	$(1, 2^+)$						
		2690.8 *8*		$(3^-, 4^+)$	1.6 *4*	1.6 *5*	m2d.fi,m1a.ff
2694	$1^{(+)}$						
2700.60 *20*							
2703.2 *10*							
		2706.3 *5*		3^-	2.4 *2*	2.7 *3*	1sdw.fi
2713.2 *6*							
2716.0 *16*	$(2^+, 3, 4^+)$						
		2725.4 *5*		2^+	0.8 *1*	0.9 *1*	1sdw.ff
2727.77 *5*	$(4,5)^-$						
2728.43 *22*	1^+						
2733.0 *12*		2733.5 *4*		$(4^+, 6^+)$	2.1 *1*	2.8 *2*	m1a.ff,m2a.ii
2738.56 *4*							
2740.16 *15*	$(4^+, 5, 6^+)$						
2740.9 *3*	1						
2741.9 *4*	2^+	2741.9 *4*	2^+		10.3 *4*	8.3 *5*	
2746.6 *3*	$(\leqslant 4)$	2747.6 *6*		(4^+)	5.2 *3*	4.6 *4*	m1a.ii
2751.9 *6*							
2757.3 *4*	$(1, 2^+)$						
		2759 *1*		1^-	0.6 *1*	0.5 *1*	m2b.hi
2763.9 *8*	$(1, 2^+)$						
2768.55 *6*							
2769.81 *15*	(5^+)						
		2770.2 *6*		6^+	0.8 *2*	1.5 *2*	m1a.ii
2778.03 *20*							
2782.9 *6*	$(1, 2^+)$						
2786.80 *7*	$(3, 4^+)$						
2788.1 *16*							
2789.2 *6*	0^+	2789.2 *6*	0^+		8.5 *2*	6.0 *6*	
2792.0 *4*	1^+						
2798.1 *3*	1^+						
2806.5 *6*							
		2809.2 *6*		2^+	1.9 *2*	1.8 *4*	1sdw.ff
2810.9 *4*							
2817.0 *4*	$(1,2^+)$						
2819.7 *4*							
2825.0 *4*	2^+	2825.0 *4*	2^+		2.3 *2*	2.2 *3*	
2826.4 *3*	$1^{(+)}$						
2833.7 *5*	$1^{(-)}$						
2842.1 *3*	0^+	2842.1 *3*	0^+		23.7 *5*	11.5 *12*	
2849.60 *5*	(4^+)						

TABLE I. (*Continued.*)

ENSDF Ref. [18]		^{170}Er$(p,t)^{168}$Er expt.					
Energy (keV)	J^π	Energy (keV)	J^π Ref. [4]	J^π present	$d\sigma/d\Omega(10^\circ)$ (μb/sr)	$\sigma_{\text{integr.}}$ (μb)	Obs.
2850.3 *4*	1^-	2850.4 *5*		1^-	3.7 *4*	2.9 *4*	1sdw.hi
2852.0 *5*							
2854.6 *4*							
2856.5 *6*	(2^+)						
		2859.1 *4*		3^-	1.4 *3*	2.1 *3*	m2a.fi
2863.6 *5*	$(1,2^+)$						
2872.2 *3*	0^+	2872.2 *3*	0^+	0^+	28.5 *5*	12.8 *15*	
2874.61 *3*	(3,4,5)						
2878.9 *4*	2^+	2878.9 *4*	2^+		5.9 *4*	5.4 *9*	
2880.6 *3*							
		2888.2 *5*		$(3^-, 4^+)$	0.9 *2*	0.7 *2*	m2d.fi,m1a.ff
2890.65 *24*							
2896.7 *3*	$(3,4^+)$						
2901.6 *3*							
2906.0 *4*	2^+	2906.0 *4*	2^+		6.5 *5*	6.3 *3*	
2907.8 *3*							
		2915.0 *5*		6^+	5.6 *3*	8.9 *6*	m1a.ii
2920.00 *24*							
		2925.7 *6*		(6^+)	1.0 *4*	1.7 *2*	1sdw.ii
2929.9 *4*	$1^{(+)}$						
2933.44 *18*	2^+	2934.1 *5*	2^+		10.4 *3*	9.0 *4*	
2942.9 *5*							
2946.6 *4*	$1^{(-)}$						
2947.4 *4*	0^+	2947.4 *5*	0^+	0^+	48.0 *6*	22.1 *19*	
2950.7 *3*							
2955.6 *8*	1						
2959.1 *10*							
2961.2 *6*	2^+	2961.2 *6*	2^+		3.1 *2*	2.6 *2*	
2969.93 *6*	$3^+, 4^+, 5^+$	2969.3 *6*		$(2^+ + 5^+)$	4.0 *3*	3.9 *2*	(doublet) 1sdw.ff,m2d.h9h9
2972.6 *7*	$(\leqslant 4)$						
2974.3 *5*	1						
2979.3 *3*	$(\leqslant 4)$						
2982.53 *10*	(3,4,5)						
2984.03 *23*							
		2987.4 *7*		1^-	1.1 *2*	0.8 *2*	1sdw.hi
2991.33 *23*	$(\leqslant 4)$						
2998.2 *4*	0^+	2998.3 *6*	0^+		3.5 *2*	2.5 *2*	
3002.4 *4*	$(1,2^+)$						
3009.0 *3*	2^+	3009.0 *3*	2^+		20.7 *4*	18.2 *4*	
3011.77 *23*	(4^+)						
3019.6 *5*	2^+	3020.0 *5*	2^+		1.9 *2*	1.5 *2*	
3026.02 *19*							
3028.6 *6*	0^+	3028.6 *6*	0^+	0^+	5.1 *2*	4.0 *2*	1sdw.ii
3030.7 *5*							
3033.9 *5*	$(\leqslant 4)$						
3042.3 *4*	2^+	3042.4 *5*	2^+		10.7 *3*	8.0 *3*	
3042.8 *3*	$3^-, 4^-, 5^-$						
3044	1						
3049.6 *4*	1^+						
3049.9 *5*	2^+	3049.9 *5*	2^+		5.0 *4*	4.8 *5*	
3055.95 *23*	2^+	3055.1 *5*	2^+		1.2 *4*	1.0 *5*	
3063.6 *3*							
3065.0 *7*	(0^+)	3065.0 *7*	~~0^+~~	1^-	1.4 *2*	1.1 *2*	1sdw.hi
3068.8 *3*							

TABLE I. (*Continued.*)

ENSDF Ref. [18]		^{170}Er(p,t) ^{168}Er expt.					
Energy (keV)	J^π	Energy (keV)	J^π Ref. [4]	J^π present	$d\sigma/d\Omega(10^\circ)$ (μb/sr)	$\sigma_{\text{integr.}}$ (μb)	Obs.
3078.0 *14*							
3081.3 *6*	2^+	3081.3 *6*	2^+		3.8 *3*	4.0 *4*	
3082 *1*	1						
3082.8 *5*	(4^+)						
3087.8 *4*		3087.0 *5*		2^+	0.8 *3*	0.9 *6*	1sdw.ff
3095.9 *6*	$1^{(-)}$						
3098.4 *6*	2^+	3098.4 *6*	2^+		2.3 *2*	2.5 *2*	
3099.42 *8*	(3^-)						
3106.6 *6*							
3111.24 *15*	$(2^+, 3, 4^+)$						
		3112.9 *6*		(3^-)	2.0 *2*	1.4 *3*	m2d.fi
3116.4 *5*	(2^+)						
3116.8		3116.8 *8*	(0^+)	(0^+)	≈0.8	1.0 *2*	m2a.ii
3118.1 *5*							
3124.40 *20*	(4^+)						
3124.5 *7*	1^+						
3127.93 *25*	$(4^+, 5, 6^+)$						
3131.9 *5*							
3137.6 *6*							
3139.6 *6*	2^+	3139.6 *6*	2^+		7.0 *3*	6.2 *3*	
3142.7 *5*							
3147.2		3147.5 *5*	~~(0^+)~~	3^-	4.3 *3*	2.6 *2*	m2a.h9i
3151.9 *16*	$(\leqslant 4)$						
3157.5 *7*	0^+	3157.5 *7*	0^+	0^+	1.0 *2*	0.6 *2*	1sdw.ii
3158.3 *16*							
		3164.7 *7*		(3^-)	0.8 *2*	0.8 *2*	1sdw.fi
3172.5 *7*	2^+	3172.5 *7*	2^+		7.5 *3*	7.0 *3*	
3181.1 *6*	1^-						
3183.7 *8*	2^+	3183.7 *8*	2^+		12.0 *3*	11.8 *3*	
3190	1^-						
3194.4 *8*	2^+	3194.4 *8*	2^+		2.6 *2*	2.4 *2*	
3198.0 *16*	$(\leqslant 4)$						
3205.2 *16*							
3208.0 *8*	$1^{(+)}$						
		3219.9 *9*		(3^-)	1.0 *1*	1.4 *2*	m2a.hi
3220	1						
3223.2 *16*	(4^+)						
3237.2 *8*	2^+	3237.2 *8*	2^+		4.9 *3*	4.5 *3*	
3238.0 *16*							
3242.6 *8*	1						
		3244.2 *10*		3^-	1.6 *2*	1.4 *3*	m2d.hi
		3262.7 *12*		4^+	0.9 *2*	1.8 *2*	m1a.ff
3269.4 *8*	2^+	3269.4 *8*	2^+		1.6 *2*	0.9 *2*	
3285.1 *16*	(4^+)						
3286.8 *8*	2^+	3286.8 *8*	2^+		3.6 *2*	4.6 *9*	
		3294.6 *8*		$(1^- + 4^+)$	2.3 *2*	2.4 *2*	(doublet) 1sdw.hi,1sdw.ff
3300.0 *7*	1						
		3305.7 *9*		(3^-)	1.8 *2*	2.6 *2*	1sdw.fi
3312.8		3312.8 *15*	~~(0^+)~~		1.0 *2*	0.6 *2*	
		3319.2 *18*			1.1 *6*	1.3 *4*	
		3326.3 *19*			0.6 *5*	0.7 *4*	
3327.3 *16*	$(\leqslant 4)$						
3335.0 *16*	$(4^+, 5^+)$						
3338.2 *6*	(2^+)						

TABLE I. (*Continued.*)

ENSDF Ref. [18]		^{170}Er(p,t) ^{168}Er expt.					
Energy (keV)	J^π	Energy (keV)	J^π Ref. [4]	J^π present	$d\sigma/d\Omega(10^\circ)$ (μb/sr)	$\sigma_{\text{integr.}}$ (μb)	Obs.
3342.0 *10*	$1^{(+)}$						
3342.9 *10*	2^+	3342.9 *10*	2^+		2.0 *2*	1.3 *2*	
3347.7 *16*							
3358.7 *6*	1^+						
3361.9 *10*	2^+	3361.9 *10*	2^+		3.8 *2*	3.9 *2*	
3370.9 *7*	(2^+)						
		3371.6 *8*		5^-	1.5 *2*	2.4 *2*	m2b.h9i
3376.6 *16*	(4^+)						
		3380.6 *8*		(0^+)	1.5 *2*	2.4 *2*	m2a.ii
3391 *1*	1^+						
		3391.1 *8*		2^+	0.9 *2*	1.1 *2*	1sdw.ff
3394.5 *16*							
3399.3 *16*	$(\leqslant 4)$						
		3404.9 *8*			1.5 *2*	1.5 *2*	
3409.7 *9*	1^+						
3415.5 *16*	$(\leqslant 4)$						
		3418.2 *10*		2^+	1.1 *2*	1.5 *2*	1sdw.ff
3429.2*10*	2^+	3429.2 *10*	2^+		5.6 *2*	5.6 *3*	
3432.0 *16*	(4^+)						
3439.6 *9*	$1^{(-)}$						
3441.7 *10*	2^+	3441.7 *10*	2^+		3.7 *2*	4.0 *2*	
3449	1						
3451.6 *10*	2^+	3451.6 *10*	2^+		1.9 *2*	2.5 *2*	
3458 *2*	1^+						
3459.9 *10*	2^+	3459.9 *10*	2^+		2.1 *2*	2.6 *2*	
3469 *2*	1^-						
3471.6 *10*	2^+	3471.6 *10*	2^+		2.5 *2*	3.1 *2*	
3475.7 *16*	$(\leqslant 4)$						
3481 *2*	1^-						
3482.6 *10*	2^+	3482.6 *10*	2^+		2.9 *2*	4.1 *2*	
3487.3 *16*							
3493.3 *10*	2^+	3493.3 *10*	2^+		10.0 *3*	10.8 *3*	
3496.4 *16*	(4^+)						
3499.3 *16*							
3504.2 *9*	1^-						
3506.3 *10*	2^+	3506.3 *10*	2^+		6.8 *2*	7.8 *3*	
3507.8 *16*	$(\leqslant 4)$						
3513.9 *16*							
3515.7 *12*	2^+	3515.7 *12*	2^+		1.9 *2*	2.5 *2*	
3516	1^-						
3521.1 *16*	$(\leqslant 4)$						
3529	1						
		3529.0 *10*	~~0^+~~	(4^+)	2.8 *2*	2.1 *2*	m1a.ii
		3535.0 *15*		(3^-)	0.5 *2*	1.3 *2*	m2a.hi
		3546.8 *15*		(3^-)	0.5 *1*	1.2 *2*	m2a.hi
3560.0 *16*							
3561.9 *12*	2^+	3561.9 *12*	2^+		2.8 *2*	2.7 *2*	
3566	1						
3569.4 *10*	0^+	3569.4 *10*	0^+	0^+	3.7 *2*	2.4 *2*	m2a.h9h9
3570.9 *16*	(4^+)						
		3577.4 *10*		(2^+)	3.1 *2*	2.8 *3*	m1a.ii
3581.1		3581.1 *10*	~~0^+~~		≈1.7	0.3 *2*	
3586.3 *10*	0^+	3586.3 *10*	0^+	0^+	3.0 *2*	1.9 *3*	m2a.h9h9
3588.0 *16*							
3591	$1^{(+)}$						

TABLE I. (*Continued.*)

ENSDF Ref. [18]		^{170}Er(p,t) ^{168}Er expt.					
Energy (keV)	J^π	Energy (keV)	J^π Ref. [4]	J^π present	$d\sigma/d\Omega(10^\circ)$ (μb/sr)	$\sigma_{\text{integr.}}$ (μb)	Obs.
3598	1						
		3599.3 *10*		2^-	0.7 *2*	1.3 *2*	m2b.ff
3606.8 *16*	($\leqslant 4$)						
		3610.2 *10*			≈0.6	0.3 *1*	
3617.6 *12*	2^+	3617.6 *12*	2^+		1.4 *2*	1.6 *2*	
3627	1						
3629.9 *12*	2^+	3629.9 *12*	2^+		1.2 *2*	1.9 *3*	
3634	$1^{(-)}$	3634.8 *10*			1.3 *2*	0.8 *3*	
		3642.8 *10*		(3^-)	0.6 *2*	0.8 *1*	m2a.hi
3643.1 *16*	($\leqslant 4$)						
3657	$1^{(+)}$						
3660.9 *16*	($\leqslant 4$)						
3663.9 *10*	0^+	3663.9 *10*	0^+	0^+	8.7 *2*	3.8 *2*	m2a.h9h9
		3671.6 *10*			2.1 *10*	1.9 *6*	
		3675.9 *10*		(3^-)	1.5 *3*	1.2 *4*	1sdw.fi
3680.1 *16*	($2^+, 3, 4^+$)						
3682.5		3682.5 *10*	~~(0$^+$)~~	2^+	4.1 *2*	2.9 *3*	m1a.ff
3696	1						
3696.7		3696.7 *10*	~~(0$^+$)~~	(3^-)	1.3 *2*	1.1 *2*	m2d.fi
3702.5 *16*	($\leqslant 4$)						
3703	1^-						
3714.9 *10*	(0^+)	3714.9 *10*	0^+	0^+	1.4 *2*	0.7 *2*	m2a.h9h9
3715.2 *16*							
3719	$1^{(-)}$						
3720.0 *15*	2^+	3720.0 *15*	2^+		2.6 *2*	2.5 *2*	
3725.2 *15*	2^+	3725.2 *15*	2^+		1.4 *2*	1.4 *2*	
3734.4 *10*	0^+	3734.4 *10*	0^+	0^+	5.0 *2*	2.0 *2*	m2a.h9h9
3737	1						
3739.0 *16*	($2^-, 3, 4^+$)						
3740.4 *15*	2^+	3740.4 *15*	2^+		2.7 *2*	2.8 *3*	
3745	$1^{(-)}$						
		3751.5 *15*		2^+	1.7 *1*	1.6 *2*	1sdw.ff
3755.4 *16*							
3760.1 *10*	0^+	3760.1 *10*	0^+	0^+	7.2 *2*	3.2 *2*	m2a.h9h9
3761.6 *16*	($\leqslant 4$)						
		3768.4 *15*		(0^+)	0.8 *1*	1.0 *2*	m2a.h9h9
3776	$1^{(+)}$						
3781.7 *16*	($4^+, 5, 6^+$)						
3789	1						
3789.5 *15*	2^+	3789.5 *15*	2^+		1.4 *2*	1.2 *2*	
		3794.1 *15*		2^+	0.9 *2*	1.0 *2*	1sdw.ff
3799.4 *16*							
3800	$1^{(-)}$						
3806	1^+						
3808.5 *15*	2^+	3808.5 *15*	2^+		3.2 *2*	2.9 *2*	
3814	$1^{(-)}$						
3817.0 *16*	($\leqslant 4$)						
3819.4 *15*	2^+	3819.4 *15*	2^+		3.8 *2*	3.8 *2*	
		3826.4 *15*			0.6 *2*	1.0 *2*	
3835.2 *16*							
		3838.0 *15*		2^+	0.5 *2*	0.8 *2*	1sdw.ff
3861.9 *15*	2^+	3861.9 *15*	2^+		1.7 *2*	1.6 *2*	
3868.7 *15*	2^+	3868.7 *15*	2^+		4.7 *2*	5.0 *2*	
3869	1						
3876.3 *15*	2^+	3876.3 *15*	2^+		2.5 *2*	2.9 *2*	

TABLE I. (*Continued.*)

ENSDF Ref. [18]		^{170}Er(p,t) ^{168}Er expt.					
Energy (keV)	J^π	Energy (keV)	J^π Ref. [4]	J^π present	$d\sigma/d\Omega(10^\circ)$ (μb/sr)	$\sigma_{\text{integr.}}$ (μb)	Obs.
3888.4 *16*		3889.1 *15*		(1^-)	1.1 *2*	0.7 *1*	m2b.hi
3895.2 *16*							
3908.3 *16*							
3912	1						
3921	$1^{(-)}$						
		3923.1 *15*		2^+	1.2 *2*	1.5 *2*	1sdw.ff
3928.9 *10*	0^+	3928.9 *10*	0^+	0^+	3.2 *3*	2.3 *3*	m2a.h9h9
3933.0 *15*	2^+	3933.0 *15*	2^+		2.1 *3*	2.1 *3*	
3960		3960.3 *15*			3.2 *3*	1.7 *2*	
3964.9 *15*	2^+	3964.9 *15*	2^+		1.3 *3*	3.1 *2*	
		3972.5 *15*		(3^-)	2.5 *2*	2.3 *2*	m2d.hi
3993		3992.5 *15*		(3^-)	5.3 *2*	6.9 *3*	m2a.hi
		4005.6 *15*		4^+	1.7 *3*	2.0 *4*	m1a.ff
		4009.0 *15*		2^+	1.5 *3*	1.9 *4*	1sdw.ff
		4020.3 *15*		(3^-)	2.0 *2*	2.1 *2*	m2d.hi
4033.5 *15*	2^+	4033.5 *15*	2^+		1.6 *2*	2.1 *2*	
		4041.9 *15*		(6^+)	0.6 *2*	1.6 *2*	m1a.ii
4055.9 *15*	2^+	4055.9 *15*	2^+		2.1 *3*	1.9 *3*	
		4060.7 *15*		2^+	1.2 *2*	1.8 *3*	1sdw.ff
4069		4069.2 *15*		2^+	0.6 *2*	0.6 *2*	1sdw.ff
4075.6 *15*	2^+	4075.6 *15*	2^+		1.9 *2*	2.2 *3*	

Graph (a) of Fig. 1 shows a general coupling scheme with seven channels for a (p,t) reaction from the ground state of spin-parity $J_i^{\pi_i}$ of a target nucleus of mass A to a state $J_f^{\pi_f}$ of the final nucleus of mass $A-2$. Each of the couplings between the seven channels figured in this graph may contribute to the cross section of the final state. The relative magnitude of these contributions depends both on the incident energy of the reaction and on the structure of the involved states. The two neutrons may be transferred either by a simultaneous process, i.e., as a pair coupled to zero angular momentum, or by a sequential process where the two neutrons are transferred one by one, through the (p,d) reaction toward states in the intermediate nucleus $A-1$ followed by a (d,t) reaction. The simultaneous transfer may be a direct, one-step process from channel 1 to channel 4 ($1 \rightarrow 4$), or by two-step processes involving the inelastic scattering of the proton and of the triton ($1 \rightarrow 2 \rightarrow 4$ and $1 \rightarrow 3 \rightarrow 4$). For reasons described below, we consider two simplified coupling schemes shown in graphs (b) and (c) of Fig. 1. The optical model potentials that describe each channel were taken from Ref. [13], except those for deuterons [in coupling scheme (b)] which come from [14]. The binding energies and the reaction Q values are supplied, and the binding energies of the transferred two neutrons are calculated such that they match the energies of the tritons for each state. Other details are given in [4]. The relative contribution of the different couplings to the cross section of a final state depends on the structure of that state.

The assignment of 0^+ and 2^+ states to a number of states in Ref. [4] was performed based on DWBA (one-step) calculations which described reasonably well the experimental angular distributions. The angular distributions for the transfer of one pair of neutrons coupled to spin 0 may depend on the transfer configurations, that is, the orbitals from which these two neutrons are removed. In principle, the real transfer may involve contributions of more than one (j_1, j_2) neutron pair (where j_i denotes the total orbital momentum of the orbital), depending on the microscopic structure of the involved states. In our case, the transferred neutrons were considered to originate from the occupied orbitals near the Fermi surface, which are mainly $2f_{7/2}$, $1h_{9/2}$, and $1i_{13/2}$ (above $N=82$) and also from the completely filled $1h_{11/2}$ orbital (below $N=82$).

The microscopic structure of the involved states is not known, but DWBA calculations have shown that the shape of the calculated angular distribution does not strongly depend on the considered j values of the transferred pair. This was explicitly shown for $L=0$ and $L=2$ (0^+ and 2^+ states, respectively) for different (j^2) neutron pairs in Ref. [4], and for $L=0,2,4$ in Ref. [5]. Consequently, the L value of analyzed states was assigned by recognizing the similarity of the experimental angular distributions with calculated ones. This process was the easiest for the 0^+ states, which have as unique features a strong peaking in the forward direction and a deep minimum around 14°–17°. Similarly, the 2^+ states show a maximum around 15° and a minimum around 30° [4]. The DWBA-calculated angular distributions show relatively stable shapes with characteristic maxima and minima for different other J^π values, as will be discussed later. These distributions also gradually change with the excitation energy of the final state. For many states one could assign L values by recognizing these patterns even if they were not perfectly displayed by the experimental data.

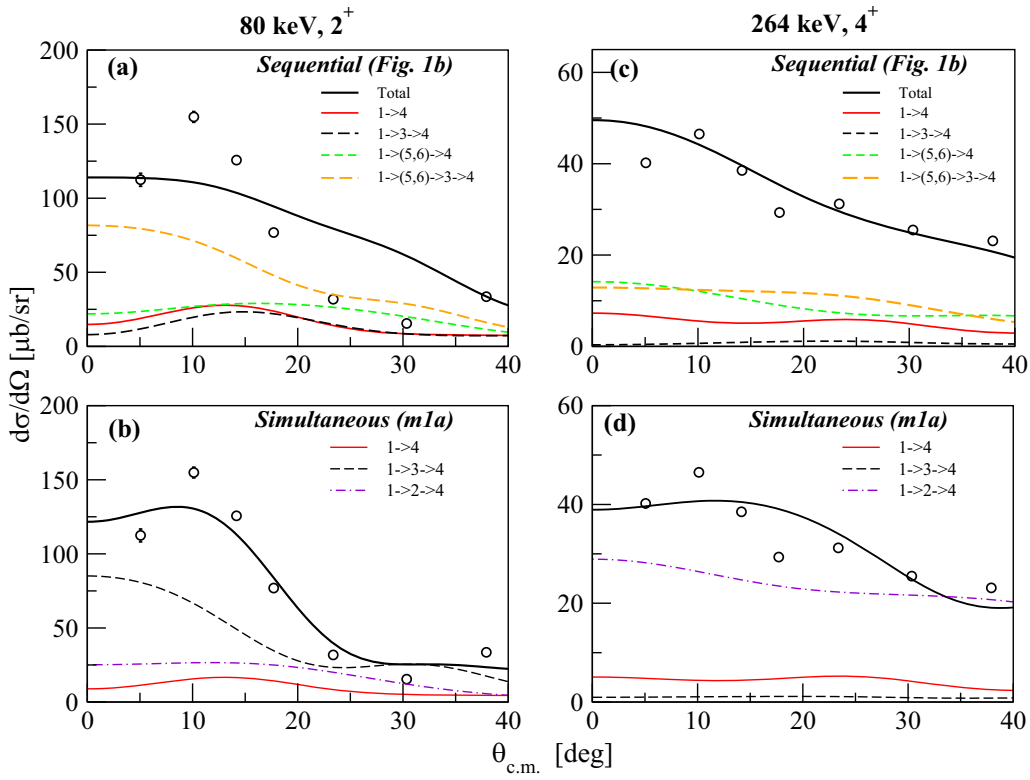

FIG. 2. Comparison of the experimental data for the 2_1^+ and 4_1^+ states of ^{168} with CHUCK3 calculations. Graphs (a) and (c): Including sequential transfer [scheme (b) of Fig. 1], with two states, $1/2^-$ and $7/2^-$, in ^{169}Er. The $S^{1/2}$ values chosen for the (p, d) transitions to these states are 1.0 and 0.5, respectively. Note that the label "Sequential" means only that sequential transfers are included (see the legend of Fig. 1). Graphs (b) and (d): Using simultaneous transfer [scheme m1a of Fig. 1(c)]. The factors used to approximately normalize the calculated curves to the experimental points are (a) 1.0, (b) 0.5, (c) 0.6, (d) 0.4. Cross sections for different reaction paths are also shown, to give an idea about the magnitude of the different amplitudes that add coherently to provide the full cross section. See text for more details.

However, there are also cases when the experimentally observed angular distributions of states of known J^π show considerable differences from the calculated one-step ones. These may be related to the presence of multistep excitations, which can be taken into account by performing CC calculations with CHUCK3, using coupling schemes such as those shown in Fig. 1.

Such an approach using the simultaneous transfer coupling schemes shown in Fig. 1(c) was demonstrated to be very useful for ^{230}Th [5], ^{228}Th [6], ^{158}Gd [7], ^{240}Pu [8], as well as for the ^{166}Er nucleus [9]. The role of the sequential transfer of the two neutrons is relatively less studied in the literature. Detailed studies of such an approach were made for the (p, t) reaction on ^{56}Fe and ^{58}Ni targets, leading to the lowest excited states of the final nuclei with magic numbers ^{54}Fe and ^{56}Ni, respectively [15,16]. When working with a complex coupling scheme, the contribution of each coupling between two channels must be correctly scaled, by introducing factors that multiply the calculated amplitude of that process. The amplitudes of the inelastic scattering channels are calculated by the code for collective excitations using the supplied nuclear deformation parameters. For the sequential transfer, the contribution of each one-neutron transfer reaction is determined by the corresponding spectroscopic factor; the calculated reaction amplitudes are multiplied by the spectroscopic amplitudes (with sign), referred to as $S^{1/2}$ in the following. For the one-neutron transfer starting from the ground state of a nucleus the experimental spectroscopic factors may have been measured, which is of great help, but, when the reactions start from excited states, these values cannot be determined experimentally and one must either rely on theoretical model calculations (when these exist) or consider them as parameters to be determined from fit. In this last case, a big disadvantage is that their number may be considerable. In the case of the simultaneous transfer [Fig. 1(c)] the factors multiplying the amplitudes of the (p, t) transfers are the corresponding quantities describing the simultaneous pair transfer, that depend on the structure of the two connected states, and are usually also regarded as parameters.

We first investigate the role of the sequential transfer in our case, in a way similar to the approach of [15] and [16]. We do this only for the 2_1^+ and 4_1^+ states of ^{168}Er, which are strongly excited and show angular distributions that deviate considerably from the one-step (DWBA) calculations. For this, we use the coupling scheme of Fig. 1(b). Figure 2 shows results of exploratory calculations with this coupling scheme.

Knowing the spin of the final state is an advantage for the investigation of the role of different couplings. We must first decide which states of ^{169}Er must be taken into consideration. In principle, one should consider all the states that

exhaust the strength of the (p, d) reaction (transitions $1 \rightarrow 5$, $1 \rightarrow 6$, etc.). Unfortunately, the experimental data are very poor in this respect. There is only one study concerning the ^{170}Er(d, t) ^{169}Er reaction at 12 MeV [17], which is limited to showing the intensities of the populated final states at two angles, 60° and 75°. The strongest populated state of ^{169}Er is the $1/2^-$ ground state, followed by the $3/2^-$, 65 keV, and $5/2^-$, 74 keV states (about ten times weaker), and two $7/2^-$ states at 177 keV (tentative spin-parity) and 224 keV, with intensities of about 0.5 of that of the ground state. All we can do in practice is to assume that the same states would be excited, in the (p, d) reaction, although on average the (p, d) reaction populates lower spin states than the (d, t) reaction. For our schematic calculations we consider two of the strongest excited states: The g.s., $1/2^-$, and the $7/2^-$ state at 224 keV. Without indication on their spectroscopic factors in the (p, d) reaction, we used trial values of $S^{1/2}$ of 1.0 and 0.5, respectively, in our calculations. For the $S^{1/2}$ values of the other couplings, in the absence of theoretical structure model calculations, we have used values of 1.0. Knowing that this is only an approximation, we also tried varying the values of the spectroscopic factors, and the sign of their amplitudes, in our test calculations, in an attempt to describe both the shape and the absolute value of the calculated cross-sections. We could not obtain very accurate descriptions of the angular distribution shapes of the two states; typical results are those shown in Fig. 2. We emphasize that these are just exploratory calculations, as the number of parameters to be adjusted is large. As an example, for coupling the state $7/2^-$ of ^{169}Er with the final state 4_1^+ of ^{168}Er, we have eight total angular momentum transfer values, and we need a value $S^{1/2}$ (with sign), for each of them. For the same reason we did not include in calculations channel 2 in the coupling scheme of Fig. 1(b). Compared to our case, the (p, t) reaction data in Refs. [15,16] benefited from the fact that they used a polarized proton beam, and thus had both cross sections and asymmetry data, the latter being rather sensitive to many details such as the signs of the amplitudes. Moreover, they had predictions for the many needed $S^{1/2}$ values from shell model calculations. Even so, they used a procedure to normalize different reaction amplitudes by introducing two additional *ad hoc* parameters. The cross-section shapes were not always greatly improved with respect to the one-step calculated ones. Surprisingly, it was found that the 2_2^+ state of ^{54}Fe is best described by a pure one-step transition [15].

In Fig. 2 we also give, besides the total cross section from the calculations, the cross sections of the different indicated reaction paths separately calculated. These separate contributions give an indication of the amplitudes (which are the square root of the cross sections) of the different coupling ways that add coherently to build up the total cross sections. We see that for these two states the contribution of the sequential transfer may be comparable to that of the direct (one-step) transfer and of the simultaneous transfer with inelastic scattering in the triton channel. In graphs (c) and (d) of Fig. 2 we show the results obtained by using the coupling scheme m1a from Fig. 1(c), based only on simultaneous neutron transfer. For both 2_1^+ and 4_1^+ states a reasonable description of the angular distribution was obtained, in particular of the forward maxima (at 10°–15°) displayed by the data. The cross sections of these states seem to have weaker contributions from sequential transfer than the assumptions in our test calculations might indicate.

For the analysis of the more than 100 states performed in this work, we have adopted coupling schemes for the simultaneous neutron transfer. As emphasized in the previous discussion, the sequential transfer is not taken into consideration because in our case there are too many unknown parameters that should be determined by comparison with the experimental data. As a result, the factors used to normalize the amplitude of each of the steps of the simultaneous transfer of the two neutrons represent effective values that may also incorporate the effect of the sequential transfer. In the case of the present ^{170}Er(p, t) ^{168}Er reaction, we find, as in Ref. [7], that the four coupling schemes shown in Fig. 1(c) are useful to characterize practically all the observed experimental angular distribution shapes. The population of final states (in ^{168}Er) is achieved by adding to the direct, one-step (p, t) transfer the coupling of inelastic and direct transfer channels: $(p, p') \rightarrow (p, t)$ and $(p, t) \rightarrow (t, t')$. A good description of a given angular distribution shape by the calculations is obtained by adjusting the values of the amplitudes required by the code for each branch (step) of the coupling scheme. The amplitudes of the two (p, t) transitions passing through the inelastic scattering channels were varied between 0 and 1 [values relative to that of the direct (one-step) coupling], and both positive and negative values were considered in the calculations. OneWe emphasize that this kind of approach was found useful in several other studies [5–9], both to confirm the known J^π for a large number of states and to assign new ones. Similarly to the one-step excitation, the way that different states are coupled to each other may depend on their microscopic structure. However, one finds also in this case a certain stability of the shape of the calculated angular distribution to the neutron orbitals considered, that allows one to recognize the $L(J)$ value of a certain state. It is remarkable that, in spite of the complexity expected for their structure, many of these states are well described by one-step (DWBA) calculations, or show relatively small deviations from such calculations.

IV. RESULTS OF THE ANALYSIS

We have performed an analysis of all the states that were not considered in the former publication [4] and have a meaningful number of measured angles, and reanalyed some of the 0^+ and 2^+ states assigned in [4]. The results of this analysis are given in Table I, where the states adopted in the ENSDF database are also shown [18]. The one-step DWBA calculations are labeled by 1sdw.ij, with (ij) denoting the transferred neutron orbital configurations, while the multistep coupled-channels calculations are specified by the label of the used coupling scheme [see Fig. 1(c)]. As many of the states with 0^+ and 2^+ assignments from [4] were adopted by ENSDF, there is some repetition of this information, which appears in both columns 2 and 4. The new J^π information is given in column 5.

By looking at Table I, one can find that for a large number of states the present analysis agrees with the J^π values

previously determined from other experiments [18], sometimes even suggesting a firm assignment instead of a tentative one. These agreements corroborate the validity of the CC approach with the CHUCK3 code. Another general observation is that most of the known states of unnatural parity were not observed in this study (Table I). This could be explained by the fact that, unlike the natural parity states, the unnatural parity ones can be populated only by two-step excitations.

A. 2^+ states and 4^+ states

A total of 66 states were assigned as 2^+ in Ref. [4], based on the good description of their angular distribution by one-step DWBA calculations. For some of these states, this assignment confirmed the value previously known from other sources [18]. In Fig. 3(a) we first show a reanalysis by CC calculations of the 80 and 2424 keV states from the older study, followed by an analysis of other 16 states, all above 2.5 MeV excitation, newly assigned as 2^+. Another new 2^+ state may exist in a possible doublet at 2969 keV excitation (see below, Fig. 6).

For the 4^+ states, we started the analysis with the 4^+_1 state at 264 keV: Figs. 2 and 3(b). For all such states found up to 2.56 MeV excitation we have been able to confirm earlier, independent assignments [18]. In most of the cases, a coupled-channels analysis was necessary to describe the observed angular distribution shape (Fig. 3). The assignment given for the 3295 keV level is only tentative, as it was found that this is may be a doublet, the shape of which can be fitted by a combination of calculated one-step transfers of 1^- and 4^+.

For the states where we show, as an example, the cross sections of the three contributing paths from the coupling scheme (3683, 1411, 2279 keV), the total cross section that fits the shape of the experimental data results from a coherent addition of the corresponding amplitudes, which are, up to the sign, the square roos of those cross sections.

B. 6^+ states and 1^- states

Part (a) of Fig. 4 displays the states assigned as 6^+. It is interesting that the states up to 2 MeV excitation, known from previous studies as 6^+ [18] (except for that at 1780 keV) need coupled-channels calculations that considerably change the shape of the one-step calculations.

Part (b) of Fig. 4 shows 1^- states. For many of them (including some with previously known 1^- assignment) the observed experimental angular distribution shows a characteristic pattern, with two maxima, at about 10° and 30°. These features show up also in some CC calculations where the two-step excitations have a smaller contribution. One should also observe that the only way to calculate 1^- states is to take the neutrons from both above and below the $N = 82$ gap, because only the combination between the orbitals of opposite parities $1i_{13/2}$ and $1h_{11/2}$ can provide a 1^- state.

C. 3^- states and 5^- states

Figure 5(a) displays the states assigned as 3^-. Many states present a maximum at about 20° which is also a characteristic

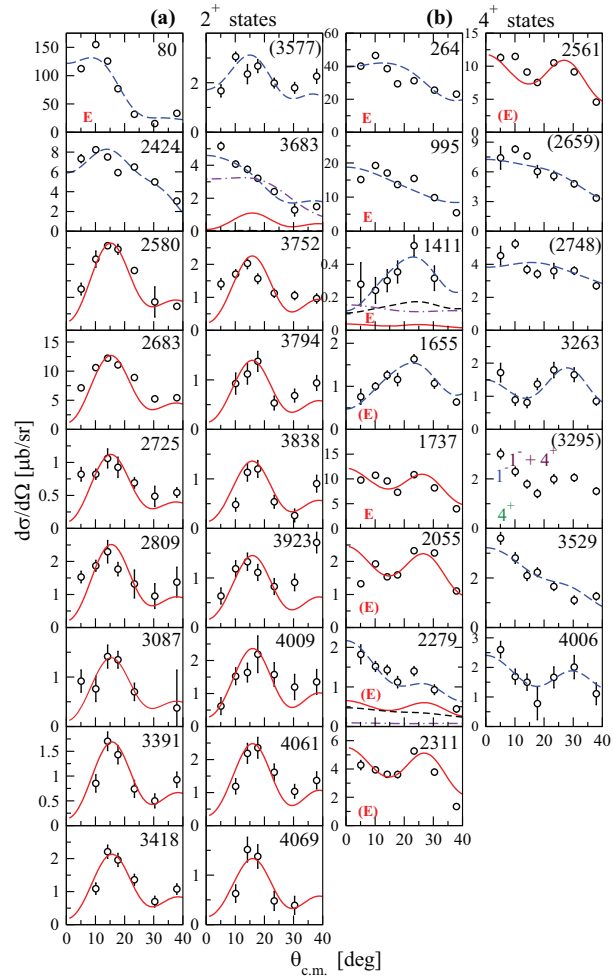

FIG. 3. Angular distributions of ^{168}Er states with (a) 2^+ and (b) 4^+ J^π assignments. Calculations with CHUCK3 are shown by curves normalized to the experimental data in order to reasonably describe the observed shapes. The energies from Table I given for each of the states were rounded off to the nearest keV of the more precise energy given in Table I. The continuous (red) curves are one-step DWBA calculations, while the dashed (blue) ones correspond to coupled-channels calculations with the coupling schemes specified in Table I. A label "E" or "(E)" in the lower-left corner of a graph denotes a firm or tentative J^π assignment, respectively, as adopted in the ENSDF database [18] for that state (see Table I). For the states with energy within parentheses our spin assignment is tentative (see also Table I). Here and in Figs. 5 and 6, for some levels that are considered to be doublets, dotted lines show the angular distributions for each of the states. Since these are incoherent, in this case the shapes should be added algebraically, with weights determined by a fit. For the 3295 keV state in graph (b) we tentatively propose a doublet of 1^- and 4^+ states, on the basis of a combination of the two one-step calculations shown. Note that in some cases, for angular distributions with relatively large difference from the one-step DWBA prediction (e.g., the 3683 or 1411 keV state), we show the cross sections separately calculated for the three coupled-channels paths (Fig. 1): One-step process, $1 \rightarrow 4$ (continuous red line); two-step $1 \rightarrow 3 \rightarrow 4$ (dashed black line) and two-step $1 \rightarrow 2 \rightarrow 4$ (dash-dotted violet line), as an indication of the magnitude of the three transfer amplitudes that add coherently to produce the total cross section for the final state.

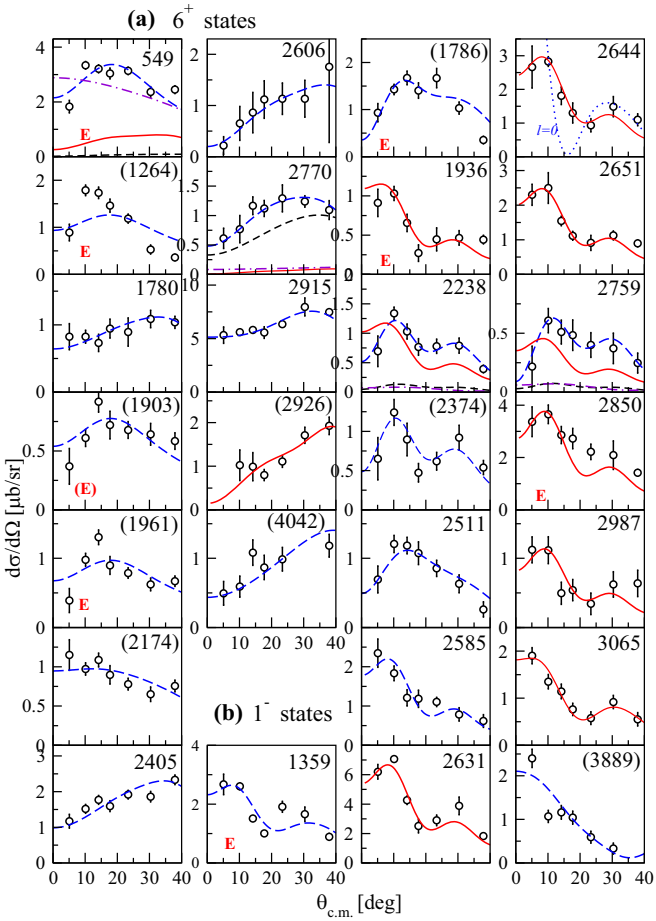

FIG. 4. The same as Fig. 3, but for the states with (a) 6^+ and (b) 1^- J^π assignments. Note that in some cases, for angular distributions with a relatively large difference from the one-step DWBA prediction (e.g., the 549 or 2238 keV state), we show the cross sections separately calculated for the three coupled-channels paths (Fig. 1): One-step process, $1 \rightarrow 4$ (continuous red line); two-step $1 \rightarrow 3 \rightarrow 4$ (dashed black line) and two-step $1 \rightarrow 2 \rightarrow 4$ (dash-dotted violet line), as an indication of the magnitude of the three transfer amplitudes that add up coherently to produce the total cross section for the final state.

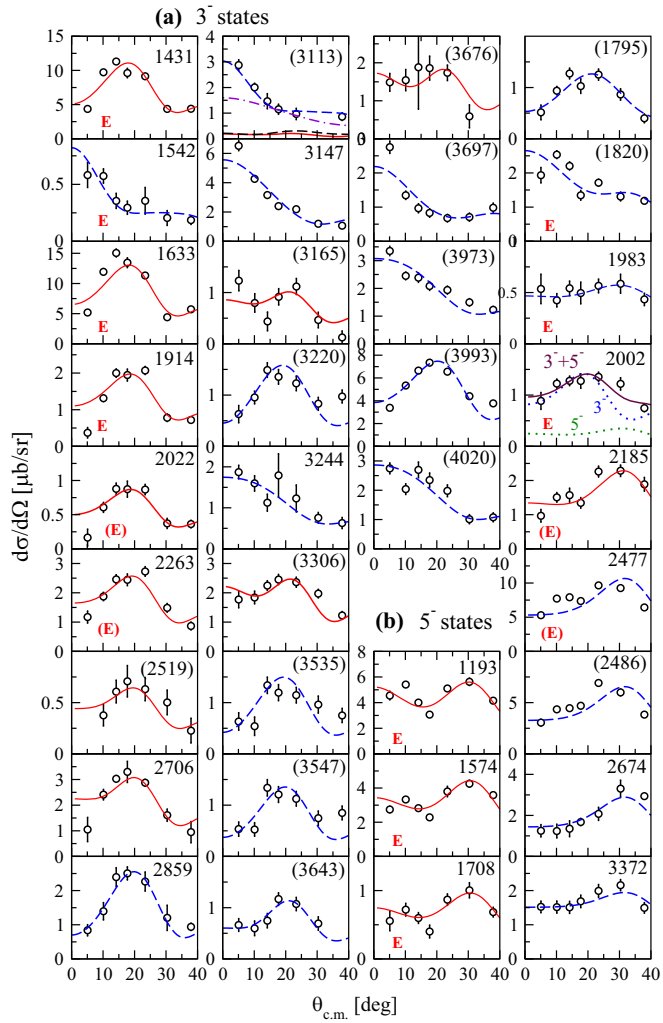

FIG. 5. The same as Fig. 3, but for the states with 3^- and 5^- J^π assignments. The 2002 keV state is assumed to be a doublet, fitted by adding one-step DWBA calculations for a 3^- state and the known 5^- states (see Table I). For the 3113 keV state we show the cross sections separately calculated for the three coupled-channels paths (Fig. 1): One-step process, $1 \rightarrow 4$ (continuous red line); two-step $1 \rightarrow 3 \rightarrow 4$ (dashed black line) and two-step $1 \rightarrow 2 \rightarrow 4$ (dash-dotted violet line), as an indication of the magnitude of the three transfer amplitudes that add up coherently to produce the total cross section for the final state.

of the one-step calculations. For the first six states of lowest energies we confirm the previous J^π assignment. The other states present various influences of the multistep excitation mechanism.

Figure 5(b) shows the states assigned as 5^-. For seven of them this assignment confirms the ENSDF one. Characteristic of the one-step mechanism of this excitation is the maximum around 30°, which is still observed in some of the states with multistep excitation influence. The angular distribution of the peak at 2002 keV is fitted by a combination of $L = 3$ and $L = 5$ curves (calculated as one-step processes) in agreement with the known closely lying levels present around this energy (see Table I).

D. 0^+ states

Figure 6(a) shows an analysis of some of the 0^+ states previously assigned in Ref. [4], as well as newly assigned states. Since 0^+ assignments are easy to make based on the strong forward peaking and the deep minimum around 17°, in Ref. [4] there were no special efforts to fit the angular distribution shape, but just a comparison with one-step calculations for a $2 \times f_{7/2}$ transfer. While for states below 2.7 MeV excitation this approach allows rather firm assignments because both the forward peaking and the position of the first minimum are reasonably well predicted, above this excitation energy there is some evolution of the experimental angular distribution shape that increases the discrepancy with the calculations. One can see (Fig. 3 of Ref. [4]) that the minimum of the angular distributions at about 17° is softened, while the one-step calculations predict a much deeper minimum. For

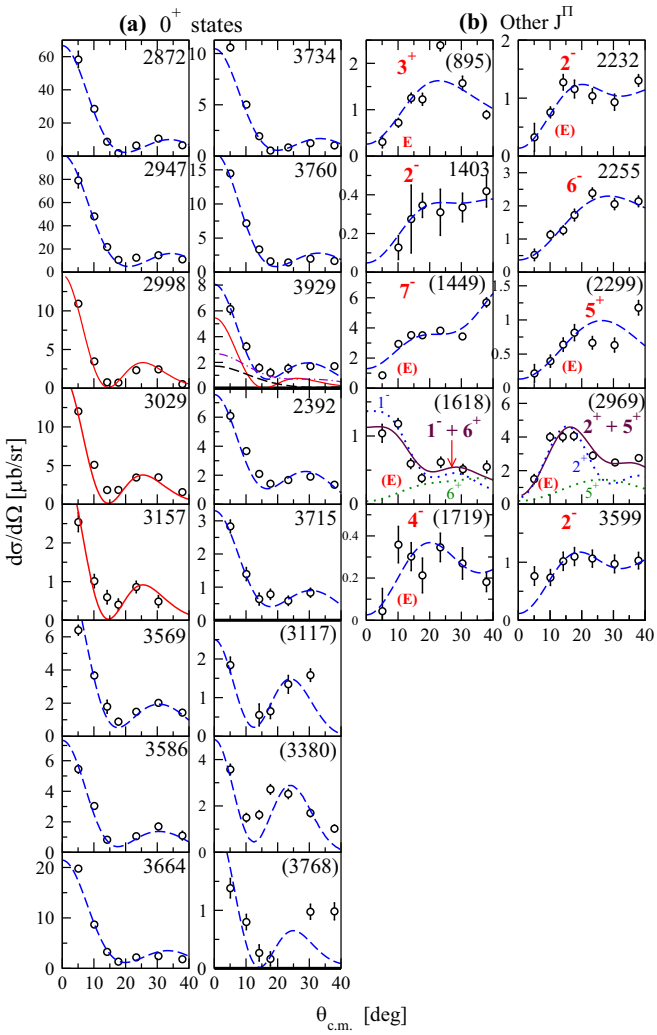

FIG. 6. Similar to Figs. 3, 4, and 5, for states of other J^π values from this study. (a) Reanalysis of states with excitation energies from 2800 to 3929 keV previously assigned as 0^+ (Fig. 3 of [4]). The two graphs following the 3929 keV state (second column) refer to the 2392 and 3715 keV states which had only tentative assignments [4]. Two other states also tentatively assigned as 0^+ (2644 and 3065 keV) are now assigned as 1^- (see Fig. 3). For the remaining three states assigned as (0^+), 3117 keV is one of a set of seven states which, due to their relatively large forward angle peaking were proposed as "possible 0^+ states" (Fig. 4 of Ref. [4]), while 3380 and 3768 keV are newly assigned. Analysis of the other states from 3117 to 3697 keV proposed as "possible 0^+ states" in [4] showed two of the states from this category (3313 and 3581 keV) could not be assigned J^π values [see part (b) of Fig. 6], while the remaining four states were assigned as follows: 3147 and 3697 as 3^- (Fig. 4), 3529 and 3683 keV as 4^+ and 2^+, respectively (Fig. 2). For the 3929 keV state we show the cross sections separately calculated for the three coupled-channels paths (Fig. 1): One-step process, $1 \rightarrow 4$ (continuous red line); two-step $1 \rightarrow 3 \rightarrow 4$ (dashed black line) and two-step $1 \rightarrow 2 \rightarrow 4$ (dash-dotted violet line), as an indication of the magnitude of the three transfer amplitudes that add up coherently to produce the total cross section for the final state. (b) Analysis of states with other J^π values. The 1618 keV and 2969 keV states are assumed as doublets, as their angular distributions could be fitted by a combination of two one-step DWBA curves (see Table I).

the states approaching 3.9 MeV excitation the assignment can even be put into question (even if the logarithmic scale used in that figure exacerbates the discrepancy in the zone of the minimum). We have reanalyzed the states between 2.87 and 3.93 MeV excitation with coupled-channels calculations, and succeeded in reproducing well the evolution in the region of the minimum; this is shown in the first column of part (a) of the figure. In Fig. 3 of [4] there were also four other states tentatively assigned [as (0^+)]: 2392, 2644, 3065, and 3715 keV. A reanalysis of these four states with CC calculations has the following results: Only the states at 2392 and 3715 have a firm 0^+ assignment (they are shown in the second column of the figure), while the states at 2644 and 3065 keV have now been assigned as 1^- (see them in Fig. 4).

There were also seven states in Ref. [4] that were characterised as "possible 0^+ states," only on the basis on their relatively strong forward peaking: 3117, 3147, 3313, 3529, 3581, 3683, and 3697 keV (Fig. 4 of [4]). These seven states have been analyzed with CC calculations, with the following results. Only the 3117 keV state remained with a tentative (0^+) assignment [see second column of Fig. 6(a)]. From the remaining six states, four of them have been assigned different J^π: 3147 keV, 3^- (Fig. 5); 3529 keV, (4^+) (Fig. 3); 3683 keV, 2^+ (Fig. 3), 3697 keV, (3^-) (Fig. 5), and two of them (3313 and 3581 keV) could not be given any assignment [graph (b) of Fig. 7]. Two other states with energies of 3380 and 3768 keV have been newly assigned as (0^+) states [the last two states shown in part (a) of Fig. 6].

In conclusion, we have reconfirmed as 0^+ all the states assigned as such between 2.87 and 3.93 MeV excitation [4]. Two of the four states tentatively assigned as 0^+, and only one of the seven "possible 0^+" states from the previous analysis [4], were reassigned as 0^+. Other J^π values were assigned to the rest of the states discussed in that paper. In addition, two other states were newly assigned as (0^+) states. In total, the number of states with firm or tentative 0^+ assignment from both our previous analysis and the present work is 27. In Table I, the firm or tentative 0^+ assignments from Ref. [4] for some of the states discussed above that were not confirmed by the present analysis have been crossed out (in column 4 of the table) and replaced by the new assignment (in column 5).

E. States with other J^π assignments

Other different J^π assignments are shown in part (b) of Fig. 6. Most of these states have unnatural parity, such as 2^-, 3^+, 4^-, and 5^+. Most of the assigned J^π values confirm the values from ENSDF [18]. The unnatural parity states have been analyzed with coupling schemes from Fig. 1 that have been adapted to them. As an example, the 2^- and the 4^- states were calculated with the m2b scheme that was truncated: Only the transitions $1 \rightarrow 2 \rightarrow 4$ were allowed, therefore these states have been described by a pure two-step process. The 895 keV, 3^+ state has been analyszd with the m2a scheme (Fig. 1), without the direct branch ($1 \rightarrow 4$). The peak at 2969 keV may be a doublet containing the known (5^+) state (Table I) and a 2^+ state (both calculated as a one-step process).

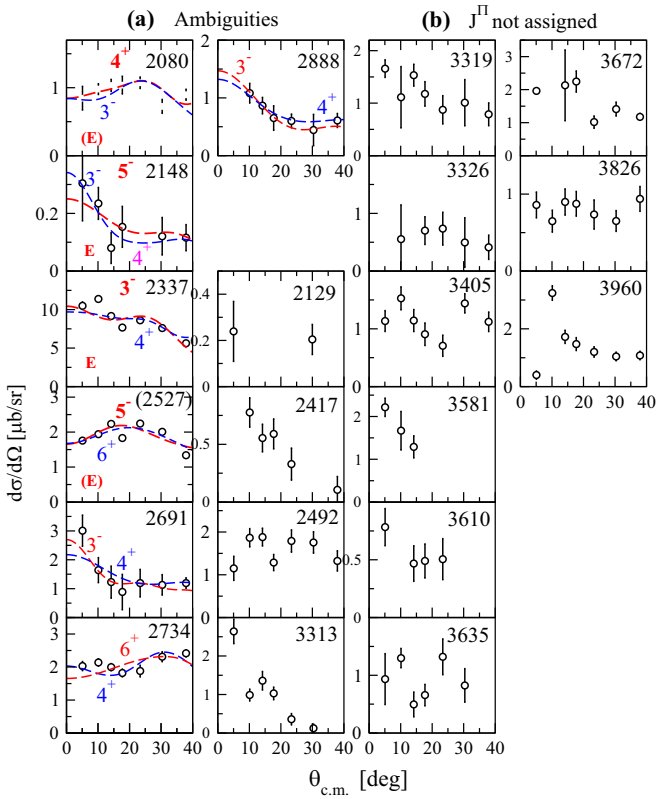

FIG. 7. (a) Some cases from our analysis where more than one J^π could be assigned to a certain state. For the first four states one of our possible assignments (marked with bold red number) coincides with the value adopted by ENSDF on the basis of other data. See also the discussion in the text. (b) Remaining states for which J^π values could not be assigned in this study.

F. Ambiguities of the analysis

During our analysis we found that sometimes it was impossible to assign a single L value (or J^π) to certain angular distributions. This is illustrated for six states in part (a) of Fig. 7. This indetermination is due to the fact that one may find two or even three calculated shapes with different L values that are very similar (e.g., 3^- and 4^+; 5^- and 6^+; etc.). For the first four states presented in Fig. 7(a), one of the possible values indicated by our analysis coincides with the J^π value from the ENSDF, therefore we have adopted that value too (see Table I).

The similarity of angular distributions calculated for different L values is more likely to appear when the angular distribution shapes are relatively flat (with a ratio between the maximum and minimum value usually less than 2). In some cases, a better definition of the experimental shape (e.g., better statistics of the points, a smoother pattern) would help one choose between the calculated curves. Nevertheless, one should be aware that an analysis with coupled channel calculations may not always be unambiguous, and for this reason in certain cases presented in the earlier subsections we adopted only a tentative J^π assignment.

G. Unassigned states

Part (b) of Fig. 7 shows the states that could not be assigned a certain J^π value in the present analysis. In some cases, the angular distribution shape was not well defined due to the small number of angles where the state was observed. In other cases, the angular distribution had large uncertainties, its shape could not be matched with any of those obtained in our trials with CC calculations, or more levels with closely lying energies may be present in the peak.

V. DISCUSSION

More than 120 states observed for the first time in the ^{170}Er(p,t) ^{168}Er reaction have been analyzed, and some states discussed in the previous publication [4] were reanalyzed, with multistep coupled channel calculations with the code CHUCK3. In more than 40 cases the assigned J^π values coincide with those adopted by ENSDF [18] based on experimental data from other sources (see Figs. 3 to 7 and Table I). The total numbers of the states assigned as 0^+ and 2^+ (including those reported in [4]) are 27 and 81, respectively. The newly added states, three in the 0^+ case and seventeen in the 2^+ case, do not significantly alter the distribution in excitation energy and in population intensity discussed in [4]. In these two cases a comparison was made in [4] with the predictions of two microscopic models: The quasiparticle-phonon model [19] and the projected shell model [20]. Both these models predict numbers of 0^+ and 2^+ states comparable to the observed ones, at least up to ≈ 3 MeV excitation.

In Fig. 8 we present a comparison between the levels observed in our (p,t) reaction experiment and the prediction of the interacting boson model 1 with s, p, d, and f bosons (spdf-IBM-1) [21]. The parameters of these calculations are given in Ref. [9], where predictions of such calculations were compared with experimental data for both ^{166}Er and ^{168}Er. The two-neutron-transfer intensities for the 0^+ states were also calculated for both these nuclei, with the simplest direct two-neutron transfer operator; while for ^{166}Er it is described reasonably well, the strong increase in ^{168}Er of the cumulative 0^+ transfer strength around 2.7 MeV is not well described (see Fig. 9 of [9]). Other transfer intensities were not calculated, because realistic $2n$-transfer operators within this model contain a large number of parameters for each transferred L value. In Fig. 8 one can see that at higher excitation energies (above $\approx$2.5 MeV) the number of calculated states drastically underestimates that of the experimentally observed states, for all J^π values evidenced in our (p,t) reaction study.

The description of the $2n$-transfer intensities remains, nevertheless, a particularly difficult issue for this nucleus. As observed in [3], the distribution of the 0^+ transfer intensity with excitation energy in ^{168}Er differs from that of the other eight nuclei from the rare-earth region. It is also different from that observed in its neighbor ^{166}Er [9]. The spdf-IBM calculations describe reasonably well the strong increase of this transfer intensity around 1.8 MeV in ^{166}Er, while they fail to describe the increase around 2.8–3.0 MeV from ^{168}Er [9].

The nucleus ^{168}Er is known as a deformed nucleus. Figure 9 displays the excitation energies of the states observed in our study as a function of $J(J+1)$, a representation that

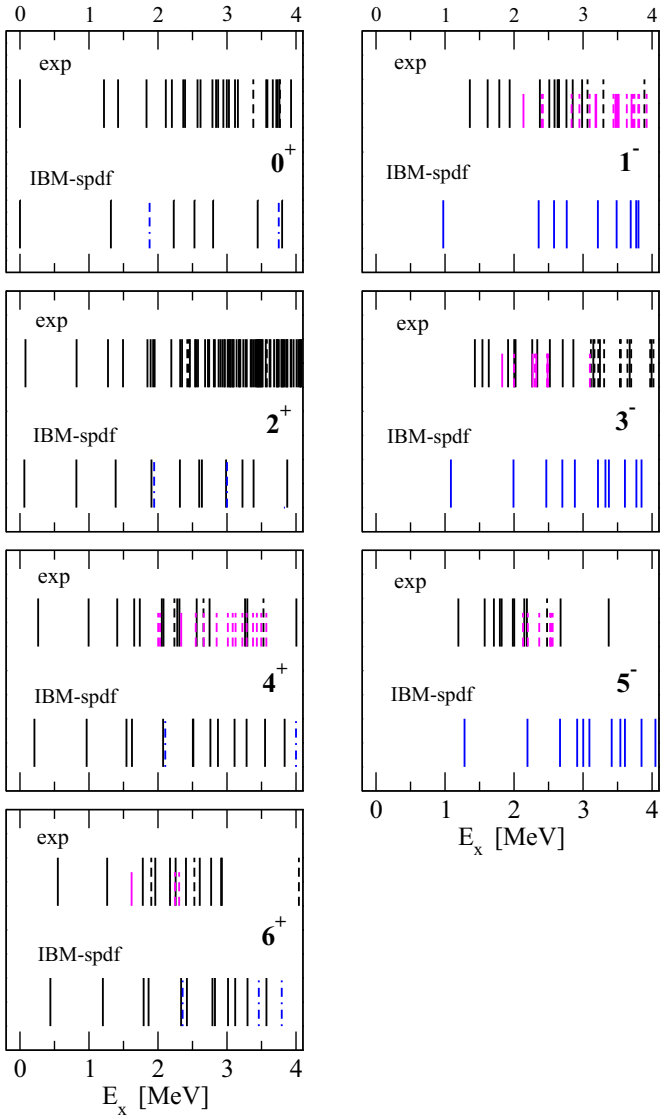

FIG. 8. Comparison between experimental states and) states calculated by spdf-IBM-1. Experimental states: Solid (dashed) longer lines denote firm (tentative assignment of states observed in this experiment, and shorter magenta lines with the same convention are states listed in ENSDF but not observed in our experiment. The spdf-IBM-1 calculated states: Dashed-dotted lines denote the two-octupole states.

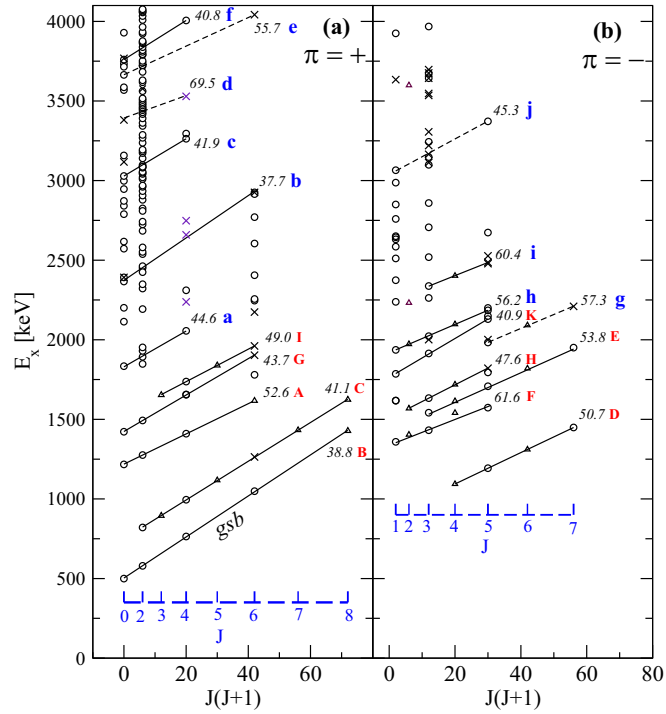

FIG. 9. Collective bands in ^{168}Er observed in this (p, t) reaction experiment. The band assignments are described in the text. The states with firm (tentative) spin assignment (Table I) are represented by circles (×'s). The two known lowest 8^+ states are shown, although they were not observed in this experiment. The bands with $K \neq 0$, the states of unnatural parity, most of them not observed in this experiment, have been added (when known [18]) as small triangles. For each identified band, the straight line shows the fit with the rotational formula, and its moment of inertia, MoI (in units $\hbar^2 \text{MeV}^{-1}$), is given in the upper part of the line. The letters next to the MoI values have the following meaning. The capital (red) letters indicate the known bands labeled by that letter in [18]. The bands proposed on the basis of the present data are labeled by small (blue) letters (see the text for their identification). Note that the ground state band (gsb) was shifted up by 500 keV to make the figure more readable.

evidences rotational bands as straight lines. In such a plot, to first order, states assigned to a band must be placed on a straight line. In addition, the intensity of their population in the reaction (here taken as the integrated cross sections from Table I) should decrease with increasing spin; the states have identical intrinsic wave functions, but their population decreases with increasing spin due to the centrifugal barrier and angular momentum mismatch. This statement refers to the natural parity states only, as the unnatural parity states have rather small cross sections. The known bands at lower energies, resulting from previous studies, five for each parity, were clearly observed. In Fig. 9 they are labeled by the (red) capital letters also used in Ref. [18] (A to K). Some other bands are proposed (a few of them tentatively) on the basis of the states observed in our reaction. In Fig. 8 they are labeled with (blue) small letters (a to j).

All the rotational bands in Fig. 9 are labeled with the value of the moment of inertia (derived from the slope of the straight lines from fits with the rotational model formula), in units of $\hbar^2 \text{MeV}^{-1}$. The ground state band (gsb) has a moment of inertia of 38.8 $\hbar^2 \text{MeV}^{-1}$, which is practically 50% of a rigid-body ellipsoid having the quadrupole deformation $\beta_2 = 0.31$ of ^{168}Er [18]. For the positive-parity bands the moment of inertia values in Fig. 8 are relatively well grouped close to the value of the gsb. For the negative-parity bands the values observed are, on average, somewhat larger than those of the positive-parity bands. Due to the relatively small number of bands assigned from the present data, one cannot deduce trends of the behavior of the moment of inertia values with excitation energy.

VI. CONCLUSIONS

In this work, a complete analysis of the states observed in the ^{170}Er(p,t) reaction at an incident energy of 25 MeV was reported. This reaction populated with measurable cross-section about 220 excited states up to an excitation energy of 4075 keV. In order to assign J^π values to these states, the large variety of observed angular distribution shapes was analyzed with coupled-channels calculations performed with the code CHUCK3, according to four different coupling schemes for simultaneous transfer of the neutrons [Fig. 1(c)].

Angular distributions for 127 states (shown in Figs. 3 to 7) were analyzed in this work (including a reanalyses of previously assigned 0^+ states [4]). Around 115 J^π assignments were proposed, 65 of them being new [for states seen only in the (p,t) reaction, or states known in ENSDF without spin assignment]. Three of these assignments differ from the previous ENSDF adopted values. For the rest of the states (except 13 states that were not assigned) the assigned J^π values (firm or tentative) corroborate those from independent studies evaluated for the ENSDF database [18].

The coupled-channels calculations prove to be a strong instrument for the characterization of the states populated in this $2n$-transfer reaction. With the J^π determinations from this work for more than 100 excited states, ^{168}Er remains one of the best-characterized nuclei below 4 MeV excitation, and thus represents a challenge for future microscopic theoretical nuclear structure models. It is difficult, however, to determine how "complete" is the level scheme of this nucleus for different spins and parities, especially in the region of high-level density above 3 MeV.

ACKNOWLEDGMENTS

D.B. wishes to thank A.I. Levon for advice on the coupled-channels calculations. We acknowledge support of this project from the Deutsche Forschungsgemeinschaft (DFG) Grant No. II C4-GR894/1-3, the Romanian Ministry for Education and Research under Contract No. CEX-05- D11-30, the DFG Grant No. 391/JO/2-3, the National Science Foundation under Contract No. PHY-0140324, and the U.S. Department of Energy under Grant No. DE-FG02-91ER-40609.

[1] S. R. Lesher, A. Aprahamian, L. Trache, A. Oros-Peusquens, S. Deyliz, A. Gollwitzer, R. Hertenberger, B. D. Valnion, and G. Graw, Phys. Rev. C **66**, 051305(R) (2002).
[2] D. A. Meyer, V. Wood, R. F. Casten, C. R. Fitzpatrick, G. Graw, D. Bucurescu, J. Jolie, P. von Brentano, R. Hertenberger, H.-F. Wirth, N. Braun, T. Faestermann, S. Heinze, J. L. Jerke, R. Krücken, M. Mahgoub, O. Möller, and D. Mücher, C. Scholl, Phys. Lett. B **638**, 44 (2006).
[3] D. A. Meyer, V. Wood, R. F. Casten, C. R. Fitzpatrick, G. Graw, D. Bucurescu, J. Jolie, P. von Brentano, R. Hertenberger, H.-F. Wirth, N. Braun, T. Faestermann, S. Heinze, J. L. Jerke, R. Krücken, M. Mahgoub, O. Möller, D. Mücher, and C. Scholl, Phys. Rev. C **74**, 044309 (2006).
[4] D. Bucurescu, G. Graw, R. Hertenberger, H.-F. Wirth, N. Lo Iudice, A. V. Sushkov, N. Yu. Shirikova, Y. Sun, T. Faestermann, R. Krücken, M. Mahgoub, J. Jolie, P. von Brentano, N. Braun, S. Heinze, O. Möller, D. Mücher, C. Scholl, R. F. Casten, and D. A. Meyer, Phys. Rev. C **73**, 064309 (2006).
[5] A. I. Levon, G. Graw, Y. Eisermann, R. Hertenberger, J. Jolie, N. Yu. Shirikova, A. E. Stuchbery, A. V. Sushkov, P. G. Thirolf, H.-F. Wirth, and N. V. Zamfir, Phys. Rev. C **79**, 014318 (2009).
[6] A. I. Levon, G. Graw, R. Hertenberger, S. Pascu, P. G. Thirolf, H.-F. Wirth, and P. Alexa, Phys. Rev. C **88**, 014310 (2013).
[7] A. I. Levon, D. Bucurescu, C. Costache, T. Faestermann, R. Hertenberger, A. Ionescu, R. Lica, A. G. Magner, C. Mihai, R. Mihai, C. R. Nita, S. Pascu, K. P. Shevchenko, A. A. Shevchuk, A. Turturica, and H.-F. Wirth, Phys. Rev. C **100**, 034307 (2019); **102**, 014308 (2020).
[8] M. Spieker, S. Pascu, D. Bucurescu, T. M. Shneidman, T. Faestermann, R. Hertenberger, H.-F. Wirth, N.-V. Zamfir, and A. Zilges, Phys. Rev. C **97**, 064319 (2018).
[9] D. Bucurescu, S. Pascu, G. Suliman, H.-F. Wirth, R. Hertenberger, T. Faestermann, R. Krücken, and G. Graw, Phys. Rev. C **100**, 044316 (2019).
[10] H.-F. Wirth, Ph.D. thesis, Technische Universität München, 2001 (unpublished), https://mediatum.ub.tum.de/602907.
[11] W. R. Stott, J. C. Waddington, D. G. Burle, and G. Lovhoiden, Can. J. Phys. **53**, 922 (1975).
[12] P. D. Kunz, Computer code CHUCK3, University of Colorado (unpublished).
[13] C. M. Perey and F. G. Perey, At. Data Nucl. Data Tables **17**, 1 (1976).
[14] W. W. Daehnick, J. D. Childs, and Z. Vrcelj, Phys. Rev. C **21**, 2253 (1980).
[15] J. H. Polane, W. F. Feix, P. J. van Hall, S. S. Klein, G. J. Neigh, O. J. Poppema, and S. D. Wassenaar, J. Phys. G **15**, 1749 (1989).
[16] M. Mahgoub, Ph.D. thesis, Technische Universität München, 2008 (unpublished), http://d-nb.info/991731786/34.
[17] T. J. Mulligan, R. K. Sheline, M. E. Bunker, and E. T. Jurney, Phys. Rev. C **2**, 655 (1970).
[18] C. M. Baglin, Nucl. Data Sheets **111**, 1807 (2010).
[19] V. G. Soloviev, *Theory of Atomic Nuclei: Quasiparticles and Phonons* (Institute of Physics, Bristol, 1992).
[20] K. Hara and Y. Sun, Int. J. Mod. Phys. E **04**, 637 (1995).
[21] F. Iachello and A. Arima, *The Interacting Boson Model* (Cambridge University Press, Cambridge, 1987).